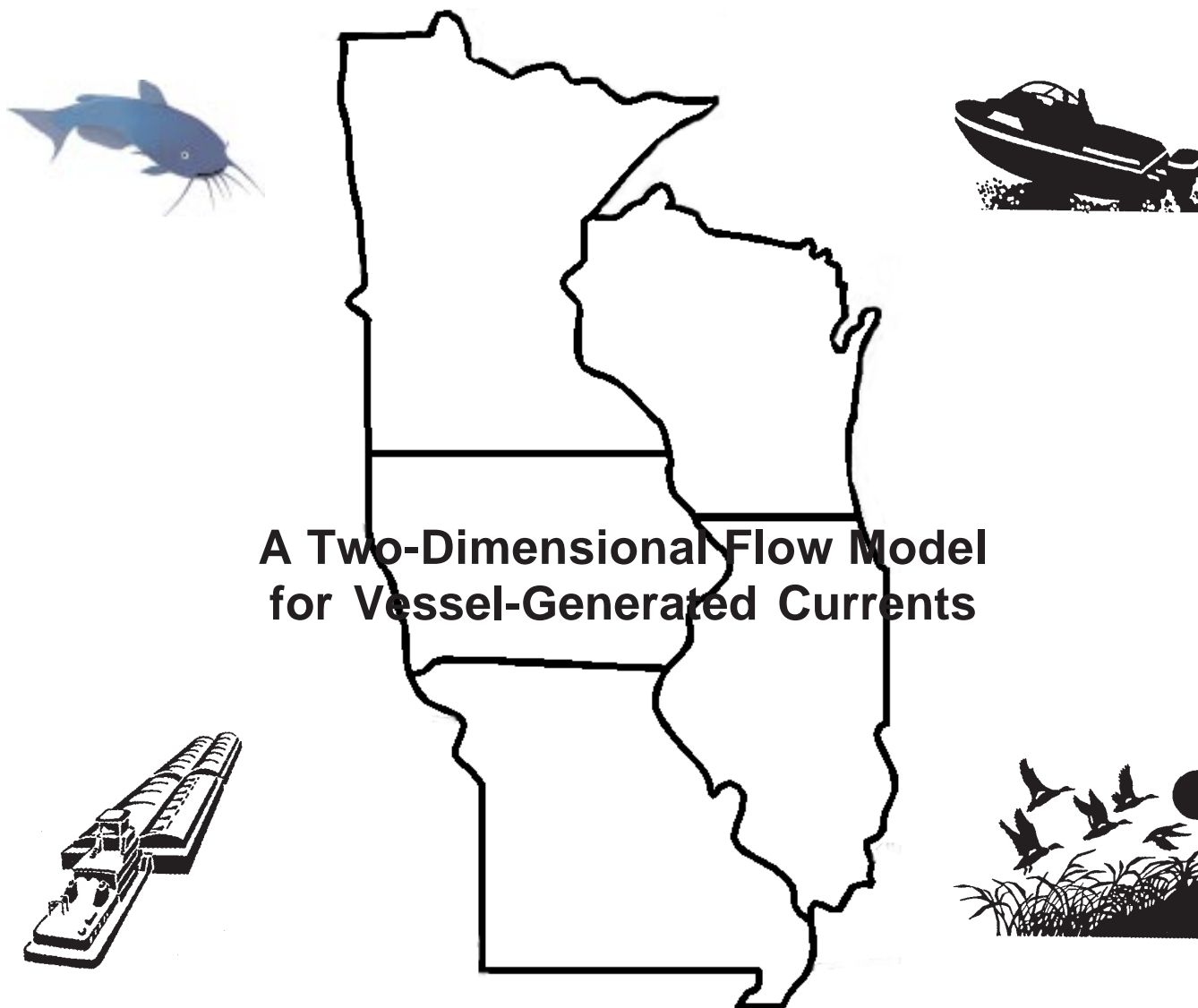


# Interim Report For The Upper Mississippi River - Illinois Waterway System Navigation Study

---



US Army Corps  
of Engineers

January 1999

Rock Island District  
St. Louis District  
St. Paul District

The contents of this report are not to be used for advertising, publication, or promotional purposes. Citation of trade names does not constitute an official endorsement or approval of the use of such commercial products.

The findings of this report are not to be construed as an official Department of the Army position, unless so designated by other authorized documents.



**PRINTED ON RECYCLED PAPER**

# **A Two-Dimensional Flow Model for Vessel-Generated Currents**

by Richard L. Stockstill, R. C. Berger

U.S. Army Corps of Engineers  
Waterways Experiment Station  
3909 Halls Ferry Road  
Vicksburg, MS 39180-6199

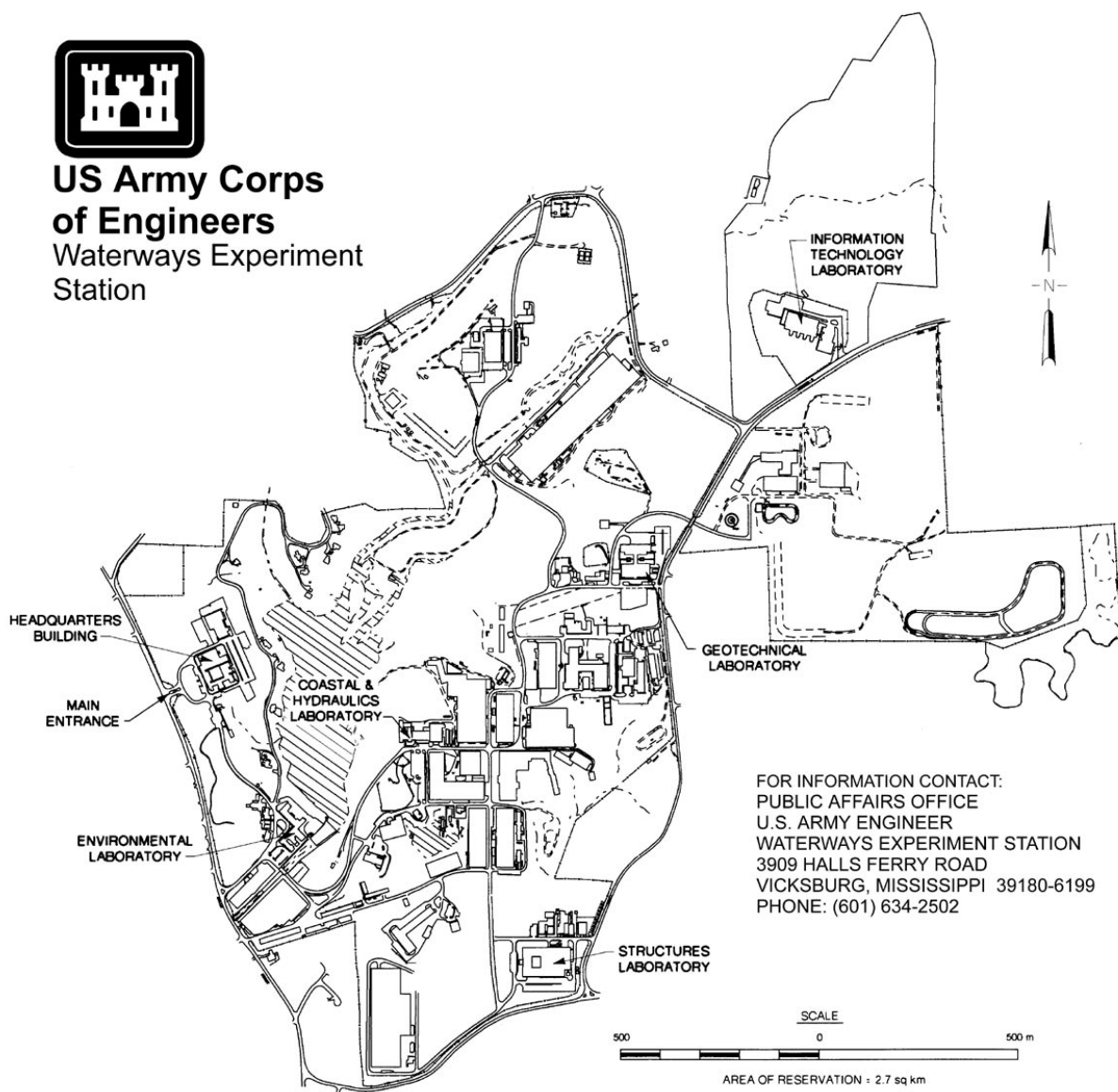
Interim report

Approved for public release; distribution is unlimited

Prepared for U.S. Army Engineer District, Rock Island  
Rock Island, IL 61204-2004  
U.S. Army Engineer District, St. Louis  
St. Louis, MO 63103-2833  
U.S. Army Engineer District, St. Paul  
St. Paul, MN 55101-1638



**US Army Corps  
of Engineers**  
Waterways Experiment  
Station



**Waterways Experiment Station Cataloging-in-Publication Data**

Stockstill, Richard L.

A two-dimensional flow model for vessel-generated currents / by Richard L. Stockstill, R.C. Berger ; prepared for U.S. Army Engineer District, Rock Island, U.S. Army Engineer District, St. Louis, U.S. Army Engineer District, St. Paul.

167 p. : ill. ; 28 cm.

"ENV report 10"

Includes bibliographic references.

1. Illinois Waterway (Ill.) 2. Tidal currents — Mathematical models. 3. Navigation. 4. Mississippi River. 5. Navigation — Mississippi River. I. Berger, Rutherford C. II. United States. Army. Corps of Engineers. Rock Island District. III. United States. Army. Corps of Engineers. St. Louis District. IV. United States. Army. Corps of Engineers. St. Paul District. V. U.S. Army Engineer Waterways Experiment Station. VI. Upper Mississippi River-Illinois Waterway System Navigation Study. VII. Title. VIII. Title: Interim report for the Upper Mississippi River-Illinois Waterway System Navigation Study.

TA7 W3499 R5U7 ENV rept.10 1999

# Contents

---

Preface.....	v
1—Introduction .....	1
Background .....	1
Purpose and Scope .....	1
Approach.....	2
2—Model Description .....	3
Governing Equations.....	3
Vessel Representation .....	5
Numerical Computational Scheme .....	6
3—Model Examination .....	9
Grid Considerations .....	9
Boundary Conditions.....	9
Model Startup.....	10
4—Model Applications .....	11
Kampsville Site ( <i>W. C. Norman</i> ).....	11
Clark’s Ferry Trip 2 ( <i>Kevin Michael</i> ).....	13
5—Screening Cases.....	15
Side Channels .....	19
Backwaters .....	20
6—Discussion and Conclusions.....	23
Discussion .....	23
Conclusions .....	23
References.....	25
Plates 1-133	
SF 298	

## List of Figures

---

Figure 1.	Discrete representation of a vessel on the numerical model computational mesh.....	7
Figure 2.	Solitary wave propagation .....	16
Figure 3.	Solitary wave traveling into a barrier .....	17
Figure 4.	Solitary wave traveling into a reservoir .....	18
Figure 5.	Geometric and hydraulic parameters describing side channels...	19
Figure 6.	Geometric and hydraulic parameters describing backwaters.....	21

# Preface

---

The work reported herein was conducted as part of the Upper Mississippi River - Illinois Waterway (UMR-IWW) System Navigation Study. The information generated for this interim effort will be considered as part of the plan formulation process for the System Navigation Study.

The UMR-IWW System Navigation Study is being conducted by the U.S. Army Engineer Districts of Rock Island, St. Louis, and St. Paul under the authority of Section 216 of the Flood Control Act of 1970. Commercial navigation traffic is increasing, and in consideration of existing system lock constraints, will result in traffic delays which will continue to grow into the future. The system navigation study scope is to examine the feasibility of navigation improvements to the Upper Mississippi River and Illinois Waterway to reduce delays to commercial navigation traffic. The study will determine the location and appropriate sequencing of potential navigation improvements on the system, prioritizing the improvements for the 50-year planning horizon from 2000 through 2050. The final product of the System Navigation Study is a Feasibility Report which is the decision document for processing to Congress.

This study was conducted in the Coastal and Hydraulics Laboratory (CHL) of the U.S. Army Engineer Waterways Experiment Station (WES). The CHL was formed in October 1996 with the merger of the WES Coastal Engineering Research Center and the Hydraulics Laboratory. The work was conducted during the period of November 1993 to September 1997 under the direction of Mr. F. A. Herrmann, Jr., Director of the Hydraulics Laboratory; and Dr. J. R. Houston, Director of CHL.

Model development was performed by Dr. R. C. Berger under the supervision of Mr. W. H. McAnally, Chief, Estuaries and Hydrosiences Division, CHL. Dr. R. L. Stockstill worked under the supervision of Mr. G. A. Pickering, Chief of the Hydraulic Structures Division, Hydraulics Laboratory; and Dr. P. G. Combs, Chief of the Rivers and Structures Division, CHL. Technical assistance in the form of consultation was provided by Dr. S. T. Maynard, Navigation Branch, Navigation and Harbors Division, CHL. The report was written by Drs. Stockstill and Berger.

At the time of publication of this report, Commander of WES was COL Robin R. Cababa, CE.

*The contents of this report are not to be used for advertising, publication, or promotional purposes. Citation of trade names does not constitute an official endorsement or approval of the use of such commercial products.*

# 1 Introduction

---

## Background

The movement of a barge train through a body of water produces a complex pattern of currents and waves. A general description of the waves and current patterns generated by a moving vessel is given by Maynard (1996). Quantification of these currents has relied on physical models and analytical descriptions. These analytical tools are primarily empirical one-dimensional models (e.g., Maynard 1996; Maynard and Siemsen 1991; and Jansen and Schijf 1953). Although empirical methods are practical for many situations, detailed analyses of specific areas are desirable. These empirical relations do not provide time-varying solutions necessary for predicting the duration of vessel-induced events. Also, spatial variations in rivers having backwaters and side channels are not modeled by these one-dimensional expressions. A two-dimensional (2-D) representation of the equations of motion provides temporal variation of the depth-averaged velocity distribution and the water-surface elevation.

## Purpose and Scope

Researchers concerned with engineering consequences and biological response to barge traffic need to know ambient flow conditions and flow field changes that are a result of vessel passage. In particular, analysis of the physical forces generated by barges navigating along a waterway requires predicting not only the changes in velocity magnitudes and directions and water-surface elevation, but also the duration of these changes. Acquisition of this information requires a time-accurate 2-D model.

The objective of this study is to develop a numerical model to quantify vessel-generated currents. Included in this report are the governing equations and assumptions made in their derivation and a brief description of the numerical model. This report also summarizes a series of numerical experiments. Finally, conclusions are made as to how the 2-D model may be used to simulate vessel-generated currents and long-period waves.

## Approach

Much attention has been given to a mathematical description of vessel-generated waves. An overview of many of the contributing researchers is presented by Stoker (1957). Stoker models vessel-generated waves as a series of impulses representing a moving pressure point. The waves generated by a moving vessel are modeled as the sum of the responses to the applied impulses. However, the application of this model to a particular vessel shape is limited by the idealized approach. Also, a method of computing not only vessel-generated waves, but also the currents resulting from vessel passage is needed. Therefore, a general method of determining spatial and temporal variations in the waves and currents generated by vessels is developed.

Flow fields containing a moving vessel are modeled by specifying a pressure field, representing a vessel hull, that is spatially varying in time. The movement of the pressure field in time is specified to represent a vessel navigating along a channel. A 2-D shallow-water model was modified to account for the effects of the imposed pressure field. The model is an extension of the finite element model HIVEL2D (Berger and Stockstill 1995; Stockstill and Berger 1994). Although HIVEL2D was developed specifically for simulation of high-velocity channels, the model was used for this study because of its numerical stability in regions of steep solution gradients.

## 2 Model Description

---

### Governing Equations

Fluid motion is modeled using the 2-D unsteady shallow-water equations. The shallow-water (or long-wave) equations are a result of the vertical integration of the equations of mass and momentum conservation for incompressible flow under the hydrostatic pressure assumption. This assumption implies that vertical accelerations are negligible when compared to the horizontal accelerations and the acceleration due to gravity. The vertical accelerations are small when the characteristic wavelength is long relative to the depth, which is why these equations are referred to as long-wave or shallow-water equations. The drawdown wave is on the order of the length of the barge train, which is much greater than the channel depth. Vertical accelerations, which result from streamline curvature, reduce the celerity of a gravity wave by the ratio (Whitham 1974):

$$K = \left\{ 1 + \left( \frac{4\pi^2 h^2}{3L^2} \right) \right\}^{-1/2} \quad (1)$$

where  $h$  is the flow depth and  $L$  is the wavelength. For the test cases presented in this report, the wavelength is approximately 10 m and the generated wave (drawdown) is about 0.2 m. Therefore,  $K$  equals 0.9974, which means that the computed wave speed is only 0.26 percent larger than wave speeds in the real system. Near the vessel the horizontal accelerations are greater, which in turn suggests that pressure gradients and vertical accelerations are more important. Although non-negligible vertical accelerations are present in the immediate vicinity of the vessel, the hydrostatic assumption is reasonable for the flow at some distance away from the vessel, which is the interest in this study.

The dependent variables of the fluid motion are defined by the flow depth  $h$ , the  $x$ -component of unit discharge  $p$ , and the  $y$ -component of unit discharge  $q$ . These dependent variables are functions of the two space directions  $x$  and  $y$  and time  $t$ . If the fluid pressure at the surface is included while the free-surface stresses are neglected, the shallow-water equations are given as (Abbott 1979):

$$\frac{\partial U}{\partial t} + \frac{\partial F}{\partial x} + \frac{\partial G}{\partial y} + H = 0 \quad (2)$$

where

$$U = \begin{Bmatrix} h \\ p \\ q \end{Bmatrix} \quad (3)$$

$$F = \begin{Bmatrix} p \\ \frac{p^2}{h} + \frac{1}{2}gh^2 - h \frac{\sigma_{xx}}{\rho} \\ \frac{pq}{h} - h \frac{\sigma_{yx}}{\rho} \end{Bmatrix} \quad (4)$$

$$G = \begin{Bmatrix} p \\ \frac{pq}{h} - h \frac{\sigma_{xy}}{\rho} \\ \frac{q^2}{h} + \frac{1}{2}gh^2 - h \frac{\sigma_{yy}}{\rho} \end{Bmatrix} \quad (5)$$

and

$$H = \begin{Bmatrix} 0 \\ gh \frac{\partial z_0}{\partial x} + \frac{h}{p} \frac{\partial P}{\partial x} + n^2 g \frac{p \sqrt{p^2 + q^2}}{C_o^2 h^{7/3}} \\ gh \frac{\partial z_0}{\partial y} + \frac{h}{p} \frac{\partial P}{\partial y} + n^2 g \frac{q \sqrt{p^2 + q^2}}{C_o^2 h^{7/3}} \end{Bmatrix} \quad (6)$$

$g$  = acceleration due to gravity

$\rho$  = fluid density

$z_0$  = channel bed elevation

$P$  = pressure at the water surface

$n$  = Manning's roughness coefficient

$C_o$  = dimensional constant ( $C_o = 1$  for SI units and  $C_o = 1.486$  for non-SI units)

And the  $\sigma$  terms are the Reynolds stresses due to turbulence, where the first subscript indicates the direction, and the second indicates the face on which the stress acts. The pressure at the free surface is zero, and the pressure at the vessel location is related to the vessel draft as:

$$P = \rho g d \quad (7)$$

where  $d$  is the vessel draft. The Reynolds stresses are determined using the Boussinesq approach relating stress to the gradient in the mean currents:

$$\sigma_{xx} = 2\rho v_t \left( \frac{\partial u}{\partial x} \right) \quad (8)$$

$$\sigma_{yy} = 2\rho v_t \left( \frac{\partial v}{\partial y} \right) \quad (9)$$

and

$$\sigma_{xy} = \sigma_{yx} = \rho v_t \left( \frac{\partial u}{\partial y} + \frac{\partial v}{\partial x} \right) \quad (10)$$

where

$v_t$  = kinematic eddy viscosity (which varies spatially)

$u = p/h$  is the depth-averaged  $x$ -component of velocity

$v = q/h$  is the depth-averaged  $y$ -component of velocity

Values of the eddy viscosity are determined empirically as a function of the local flow variables (Rodi 1980; Chapman and Kuo 1985):

$$v_t = \frac{Cn}{h^{1/6}} \sqrt{8g(p^2 + q^2)} \quad (11)$$

where  $C$  is a coefficient that varies between 0.1 and 1.0.

## Vessel Representation

The coordinates of the vessel center  $S$  are moved during each time-step in accordance with the vessel sailing speed and direction as:

$$S = S_0 + \Delta S \quad (12)$$

where  $S_0$  is the initial location of the vessel corners, and  $\Delta S$  is computed as:

$$\Delta S = \begin{cases} \frac{1}{2}at^2 & 0 \leq t \leq t_s \\ \frac{1}{2}at_s^2 + at_s(t - t_s) & t \geq t_s \end{cases} \quad (13)$$

where  $a$  is the specified vessel acceleration, and  $t_s$  is the time at which the vessel reaches a constant velocity ( $at_s$ ).

After the vessel center location is determined, the vessel corner coordinates are calculated from the vessel length and width. The induced pressure field resulting from the vessel draft is applied to every node within the vessel boundary, as illustrated in Figure 1. The computational mesh is constructed to apply pressure gradients across the bow, stern, and each side boundary to maintain the appropriate blockage area (vessel cross-sectional area).

## Numerical Computational Scheme

The finite element approach used is a Petrov-Galerkin formulation, which is a combination of the Galerkin test function and a non-Galerkin component to control oscillations (Berger and Stockstill 1995).

$$\sum_e \left[ \int_{\Omega_e} N_i^* \left( \frac{\partial \tilde{U}}{\partial t} + \frac{\partial \tilde{F}}{\partial x} + \frac{\partial \tilde{G}}{\partial y} + \tilde{H} \right) d\Omega_e \right] = 0, \text{ for each } i \quad (14)$$

where the subscript  $e$  identifies a particular element that is part of the domain  $\Omega$ , the subscript  $i$  indicates a particular test function, and the  $\sim$  symbolizes a discrete value of the variable. The finite element approximation  $\tilde{U}$  for the solution of the governing equations is given as:

$$\tilde{U} = \sum_j N_j U_j \quad (15)$$

where  $N_j$  are the bilinear basis functions and  $U_j$  are the nodal values of the solution. The Petrov-Galerkin test function, which consists of a combination of even and odd functions, is written as:

$$N_i^* = N_i \mathbf{I} + N_i' \quad (16)$$

where  $N$  is identical to the basis function,  $\mathbf{I}$  is the identity matrix, and:

$$N_i' = \beta \left( \Delta x \frac{\partial N_i}{\partial x} \hat{A} + \Delta y \frac{\partial N_i}{\partial y} \hat{B} \right) \quad (17)$$

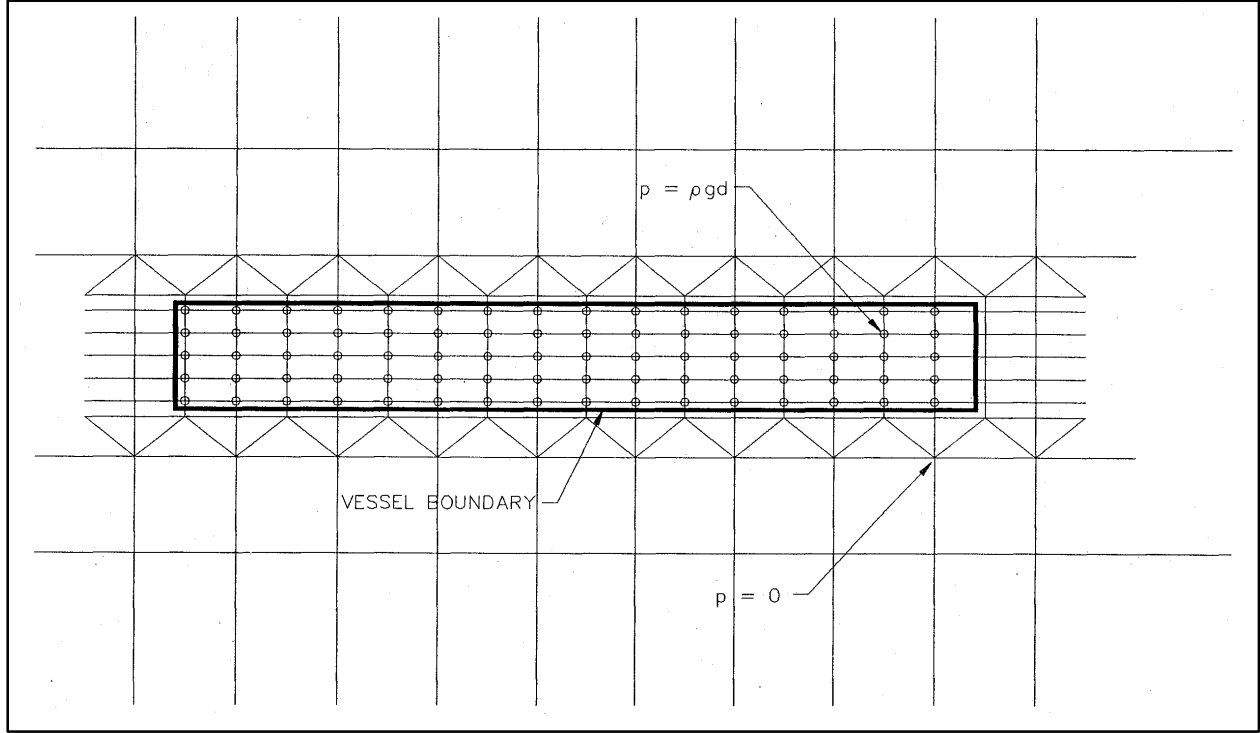


Figure 1. Discrete representation of a vessel on the numerical model computational mesh

is the stabilizing component added to the Galerkin test function. Here,  $\beta$  is a dimensionless number between 0 and 0.5,  $\Delta x$  and  $\Delta y$  are the representative element lengths (Katopodes 1986), and  $\hat{A}$  and  $\hat{B}$  are functions of the flow characteristics (Berger and Stockstill 1995; Berger 1993).

To facilitate the specification of boundary conditions, the weak form of the equations is developed using integration by parts. The weak form of the equations is given as:

$$\sum_e \left[ \int_{\Omega_e} \left( N_i^* \frac{\partial U}{\partial t} - \frac{\partial N_i}{\partial x} \mathbf{F} - \frac{\partial N_i}{\partial y} \mathbf{G} + N_i' \mathbf{A} \frac{\partial U}{\partial x} + N_i' \mathbf{B} \frac{\partial U}{\partial y} + N_i^* \mathbf{H} \right) d\Omega_e \right. \\ \left. + \oint_{\Gamma_e} N_i (\mathbf{F} n_x + \mathbf{G} n_y) d\Gamma_e \right] = 0, \text{ for each } i \quad (18)$$

where  $(n_x, n_y) = \hat{\mathbf{n}}$  is the outward unit vector normal to the boundary  $\Gamma_e$ , the symbol  $\sim$  has been omitted for clarity, and the variables are understood to be discrete values. The natural boundary conditions given in the weak statement are applied to the sidewalls to enforce no mass or momentum flux through these

boundaries. A partial slip condition is implemented at these boundaries, which allows a velocity along the wall but imposes a friction stress.

Difference equations are used to approximate the temporal derivative of the set of variables  $\mathbf{U}_j$ :

$$\left( \frac{\partial \mathbf{U}_j}{\partial t} \right)^{k+1} \approx \frac{(1 + \alpha)}{2\Delta t} (\mathbf{U}_j^{k+1} - \mathbf{U}_j^k) + \frac{(1 - \alpha)}{2\Delta t} (\mathbf{U}_j^k - \mathbf{U}_j^{k-1}) \quad (19)$$

where  $j$  is the nodal location and  $k$  is the time-step. An  $\alpha$  equal to 1.0 results in a first-order backward difference approximation, and an  $\alpha$  equal to 2.0 results in a second-order backward difference approximation to the temporal derivative. This implicit description of the nonlinear equations is solved using the Newton-Raphson method of iteration. The derivatives comprising the Newton-Raphson Jacobian are determined analytically, and the Jacobian is updated at every iteration.

## 3 Model Examination

---

Initially, numerical experiments were conducted to determine the optimum manner of simulation. Several runs were made of a hypothetical channel configuration to assess the effects of computational mesh refinement, boundary conditions, and vessel acceleration.

### Grid Considerations

Simulations were made to determine the grid density required to adequately resolve the flow field. Basically, the vessel geometry sets the resolution of the finite element mesh. Particular attention was paid to the mesh along the vessel path where the flow gradients are largest. Typically, the vessels modeled are tow configurations three barges wide (about a 32.0-m-wide hull).

Initially, grids were composed of two elements across the 32-m-wide vessel. These results, shown in Plate 1, were compared with those obtained for three elements across the vessel. This process was continued until additional resolution did not significantly change the solution. Plate 1 shows that the three- and four-element results are essentially the same.

Longitudinal resolution was found to be adequate when two elements were used to represent the length of each barge, 59.4 m. Thus a longitudinal-to-transverse aspect ratio of 3.7 was used for each element representing the sailing line. Time-step size was chosen so that the vessel moved one element longitudinally in each time-step.

### Boundary Conditions

The first experiments simulated cases with no ambient flow, so each of the four boundaries was treated as no-flux boundaries. Early results revealed that a wave was generated at the startup of the simulated tow. This “startup wave” traveled at the speed of a gravity wave,  $c = (gh)^{1/2}$ , in front of and away from the vessel, because the wave speed was larger than the vessel speed. When the startup wave reached the opposite end of the domain, this no-flux boundary reflected the wave. The model runs were supposed to simulate a vessel that had been traveling for quite

some time, so that the results would be free from startup noise. In order to reduce the presence of the reflected startup wave in the results, the boundary in the direction of the vessel travel was treated as an outflow boundary. A tailwater elevation equal to the initial water-surface elevation was applied as the boundary condition at the outflow boundary.

## Model Startup

The model allows the user to specify a linear acceleration from an initial vessel speed of zero to the steady vessel speed. Experiments were conducted to determine the sensitivity of results to the model startup rate. Model results using various simulated vessel accelerations were compared. These comparisons were of time-history plots of velocity and water-surface elevations at a point in the flow field.

Three runs were made to assess the impact that the initial acceleration of the vessel had on the equilibrium results. The acceleration time is defined as the time required for the vessel, starting at rest, to reach the final velocity of 10 fps (3.048 m/sec). All accelerations were specified as linear. The flow field solutions for acceleration times of 97.5 sec, 9.75 sec, and 195 sec were compared. Time-history graphs for each run indicate that an equilibrium state relative to the vessel was reached. The effects of vessel startup are best seen by comparing variables at a given spatial location for various acceleration times. Plate 2 is a time-history of the water-surface elevation and the longitudinal velocity at a particular point located at the top of the channel side slope. It is evident from these plots that the acceleration time (within the range evaluated) did not appreciably affect the equilibrium results. Each of the three numerical experiments produced essentially the same return current and drawdown.

## 4 Model Applications

---

Additional numerical experiments were conducted to evaluate the ability of the 2-D model to simulate the currents and waves generated in the field by a vessel navigating along a waterway. Two sites were selected for comparison. The Kamps-ville and Clark's Ferry sites were chosen because both prototype and physical model data are available for comparison. The field data sets used for the model evaluation were obtained by the Illinois State Water Survey (Bhowmik, Soong, and Xia 1993, 1994). The laboratory data are a product of the physical forces study conducted at the U.S. Army Engineer Waterways Experiment Station. These two studies provided excellent data sets with which the numerical model could be evaluated.

### Kampsville Site (*W. C. Norman*)

The first site investigated was the Kampsville site, located on the Illinois Waterway System at river mile 35.2. Details of the field observations are reported in Bhowmik, Soong, and Xia (1993). The effects of barges navigating through the Kampsville site were further documented in a laboratory environment by Maynard and Martin (1997). This investigation employed a 1:25-scale model of the Kampsville site with various tow arrangements and navigation conditions.

The Kampsville site data set used for this report is for a 3-wide by 4-long down-bound barge train towed by the M.V. *William C. Norman*. This vessel, which traveled at 2.9 m/sec, was 237.7 m long by 32.0 m wide, and drafted at 2.74 m. The river flow rate was 628 m<sup>3</sup>/sec with a 4.67-m depth at the thalweg. A sketch of the river cross section at Kampsville is illustrated in Plate 3 in which the sailing line is referenced to the thalweg. The cross-section sketch also shows the location of Bhowmik's gauges. Model parameters used in the simulations are listed in the following tabulation.

The numerical model computational mesh of the laboratory test facility is shown in Plate 4. The mesh consisted of 2069 nodes and 2434 elements. Both triangular and quadrilateral elements were used. The increased longitudinal resolution on the side slopes was in the vicinity of the physical model test section where the data acquisition gauges were located.

Model Parameter	Value Used for Simulations	
	Physical Model	Prototype
$g$ , m/sec <sup>2</sup>	9.81	9.81
$n$	0.010	0.025
$C$	0.1	0.1
$A$ , m/sec <sup>2</sup>	0.036082	0.0047134
$T_s$ , sec	16.13	615.26
$\beta$	0.25	0.25
$\alpha$	1.5	1.5
$\Delta t$ , sec	1.025	5.14

The selection of appropriate parameters for the model was made from hydraulic experience and not as an adjustment to match the flume results. The numerical model was run independently from the flume testing, in a "blind" test. The vessel speed was 0.582 m/sec. A Manning's  $n$  value of 0.010 was assumed for the smooth concrete and the epoxy-painted plywood. This value is in agreement with  $n$  values presented in Brater and King (1976).

Velocities are compared in the x-direction (parallel to path of tow) and in the y-direction (perpendicular to tow motion). Tow motion is from right to left in Plate 4. Positive velocities in the x-direction are in the same direction as the tow motion. That is, return currents are taken as negative x-direction velocities. The y-direction velocities are positive in the direction away from the vessel. The timing scale is such that zero is the time when the bow reaches the station where the probe is located.

Time-histories of computed velocities are compared with those measured in the flume in Plates 5-10. The flume data are a 1.0-sec moving average of the raw data. Generally, the  $x$  velocity compares well, though the maximum values are somewhat low. The  $y$  velocity compares quite well as the bow passes and the currents are away from the vessel (in the positive direction). Near the stern, where the currents are toward the vessel (in the negative direction), the  $y$ -component currents are consistently high in the numerical model. The results suggest that the level of turbulence chosen in the numerical model may be too low. The turbulence level could be increased by selecting a value of  $C$  larger than 0.1.

The computed and measured velocities at probe 6V (Plate 10), which is located near the top of the right side slope, did not compare as well. Differences between models could be attributed to instrument placement or bathymetry variations near the bank in the physical model. Numerical results may differ due to several possibilities including insufficient resolution near the side boundaries, an inadequate turbulence model for the low Reynolds numbers found in the physical model, or an inappropriate 2-D assumption in an area where there is a potential for vertical motion.

Wave heights relative to the still water level are shown in Plates 11 and 12. The computed values are in reasonable agreement with those measured in the flume, with the exception of the latter portion of the time-history when the vessel has passed the test section. The numerical model did not simulate a tow deceleration, whereas the flume tow was decelerated. Perhaps this explains the difference in the wave rebound after the vessel passes the test section. Attention is focused on the drawdown at wave rod 1W (Plate 11), approximately 0.5 vessel width from the vessel. The maximum value on the drawdown portion of the curve is captured by the numerical model.

Evaluation of the hydrodynamic model was continued by comparison with field data (Bhowmik, Soong, and Xia 1993). The model parameters for these runs are shown in the earlier tabulation. Details of the numerical model computational mesh in the vicinity of the data gauges are illustrated in Plate 13.

Model comparisons with flume and field data are shown in the time-histories of longitudinal and lateral velocities at a particular point within the river (Plates 14-19). Plate 20 illustrates the drawdown generated by the barge train. In Plates 14-20, zero time corresponds to the bow of the vessel crossing the river section. Plate 21 illustrates the distribution of maximum return currents across the channel. The numerical model accurately reproduces the maximum return current at distances greater than about two vessel widths from the sailing line. Discrepancies in the immediate vicinity of the vessel result from the hydrostatic pressure assumption of the model. Vessel movement generates significant vertical accelerations in and adjacent to the vessel path. However, horizontal momentum is conserved, and the model accurately simulates the far field where the pressure distribution is hydrostatic.

## **Clark's Ferry Trip 2 (*Kevin Michael*)**

The data set used in this report from the Clark's Ferry site, Trip 2, is of conditions resulting from a 3-wide by 4-long downbound barge train towed by the M.V. *Kevin Michael*. This particular site was selected for model examination because of the presence of numerous dikes and because field data (Bhowmik, Soong, and Xia 1994) and physical model data (Maynard and Martin 1998) are available for comparison. Plate 22 shows the river cross section of this site. A typical reach of river containing a dike field was simulated (Plate 23). The barge train was 237.7 m long by 32.0 m wide and drafted at 2.74 m. The vessel was traveling downstream at 2.31 m/sec. The river discharge was 673 m<sup>3</sup>/sec. Model parameters are listed in the following tabulation. Plate 24 shows a representative portion of the computational mesh in the vicinity of the dike field.

Time-histories of velocities are provided in Plates 25-28. The flow in the vicinity of the dike field is considerably different from that observed at the prismatic channel of the Kampsville site. Generally, the model-computed maximum change in velocity from the ambient current is in agreement with the field measurements. However, the model-computed ambient currents do not agree as well with the

Model Parameter	Value
$g$ , m/sec <sup>2</sup>	9.81
$N$	0.025
$C$	0.1
$a$ , m/sec <sup>2</sup>	0.00292, 0
$t_s$ , sec	791.6364
$\beta$	0.25
$\alpha$	1.5
$\Delta t$ , sec	2.0

ambient currents measured in the field. Maximum return currents as distributed across the channel are shown in Plate 29. Although the physical model and field data are somewhat limited, the numerical model seems to reasonably predict the return currents at a distance of about 2.5 vessel widths from the sailing line.

## 5 Screening Cases

---

This section contains several example runs for two general cases. One is termed a backwater example. This is a simple branch off the main stem channel that is a dead end. That is, it has only the one connection to the main channel and the other end is closed. The second example type is a side channel. This is a branch off the main stem that re-enters the main channel. This could represent the conditions in the shore side channel behind an island. The results of these runs appear complicated but, at least qualitatively, are made up by the superposition of rather simple descriptions.

First, consider a small solitary wave traveling along an initially stagnant, long uniform channel of constant depth  $H$ . A positive wave (the displacement is above the flat water surface) will generate velocity in phase and in the direction of wave travel. This positive solitary wave schematic is shown in Figure 2a. A negative wave (a depression in the water surface), on the other hand, will generate velocity that is in phase but in the opposite direction of the wave travel (Figure 2b).

The example channels in this report are not infinitely long, but they have either a closed end or a junction with the main river. Extension of the simple infinite channel concept must include these closed-end and main-river-junction boundary types. When a wave hits a solid barrier, a positive reflection occurs. That is, if a positive displacement wave is traveling to the right into a barrier, a reflected wave that is also positive and traveling to the left will result. The superposition of the waves at the barrier produces a velocity of zero but the wave height is amplified, as shown in Figure 3. If there is no damping, the wave amplitude at the barrier will be double the initial wave amplitude. The junction of the channel with the main river constitutes an abrupt expansion. The water surface at the channel inlet will tend to remain at a constant height, as a reservoir does. A wave impinging on a reservoir will produce a negative reflection. The reflected wave will have the opposite displacement and will be traveling in the opposite direction of the original incident wave. The currents of the incident and the reflected waves are in the same direction. At impact with the reservoir, the superposition of the incident and reflected waves results in a constant water-surface elevation but an amplified velocity magnitude, as depicted in Figure 4.

These descriptions are qualitative in that they consider no friction, viscosity, or reflection losses; however, they are useful in interpreting the model results. These conceptual models need to be related to the specific problem of a vessel passage in

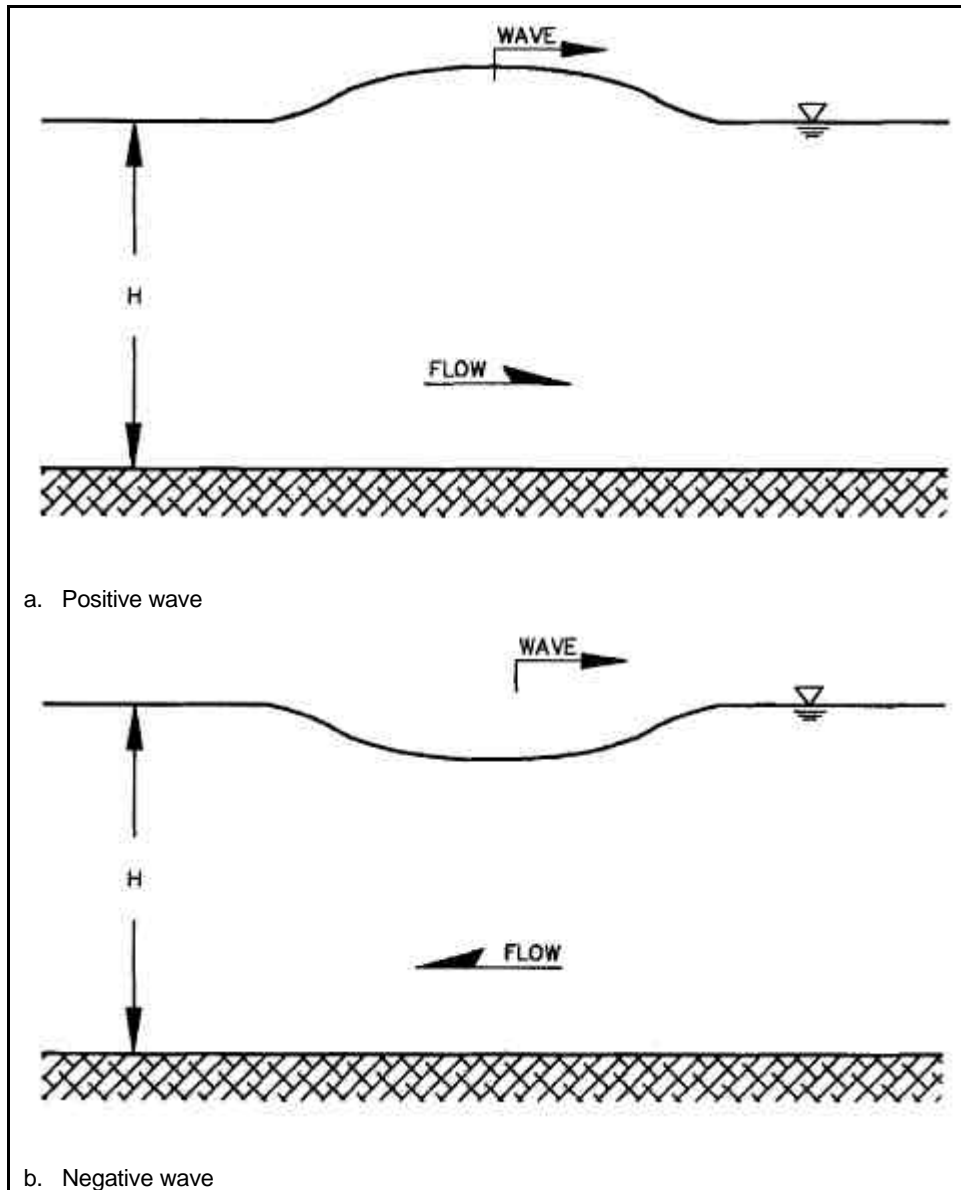


Figure 2. Solitary wave propagation

the main river. The moving vessel develops a drawdown that travels beside and with the vessel. This depression in the water surface will then propagate into the backwaters and side channels, resulting in an exchange of volumes between the channel and these off-channel features. This vessel-generated water-surface depression will produce a drawdown at the inlet of a side channel or backwater, and a depression wave that travels through these channels. This wave has a speed, or celerity, of roughly  $(gH)^{1/2}$ .

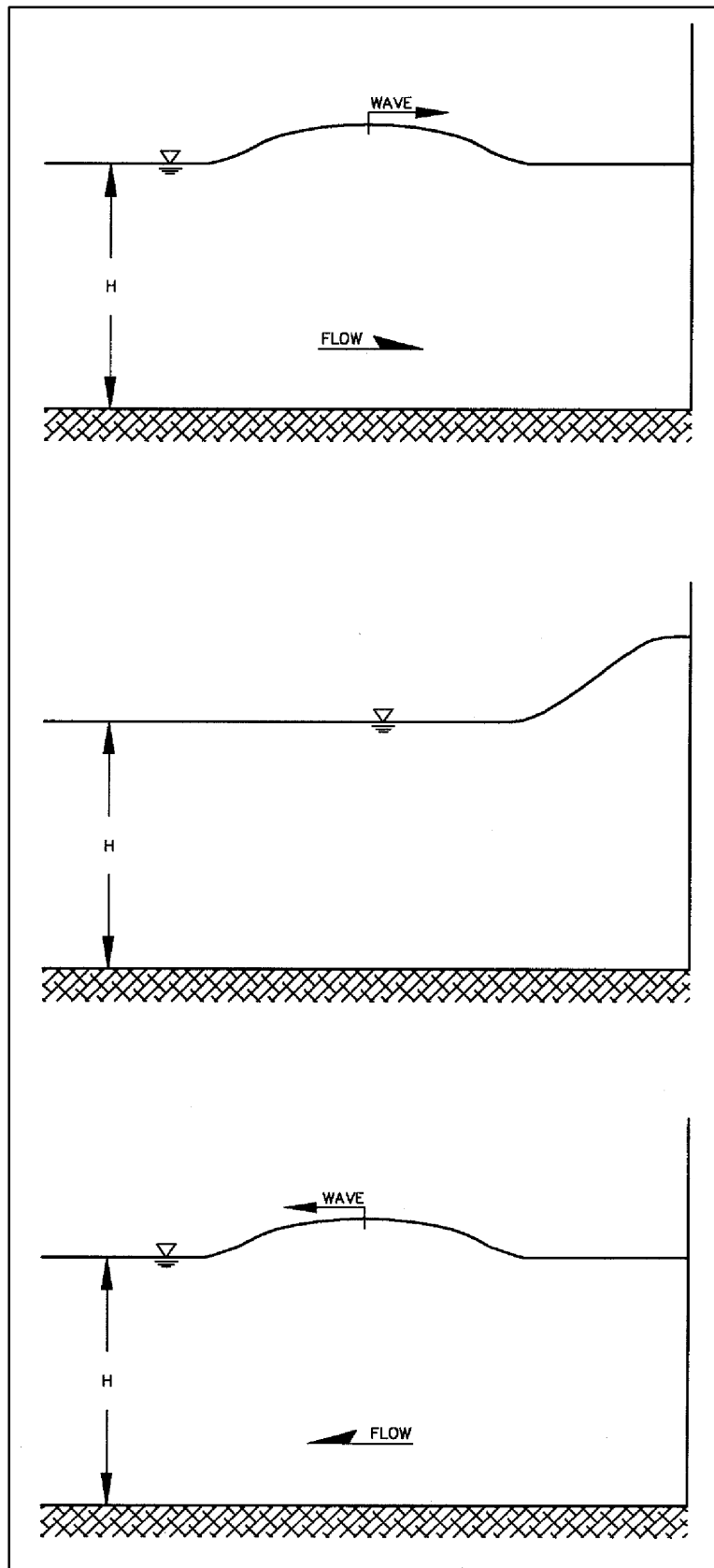


Figure 3. Solitary wave traveling into a barrier

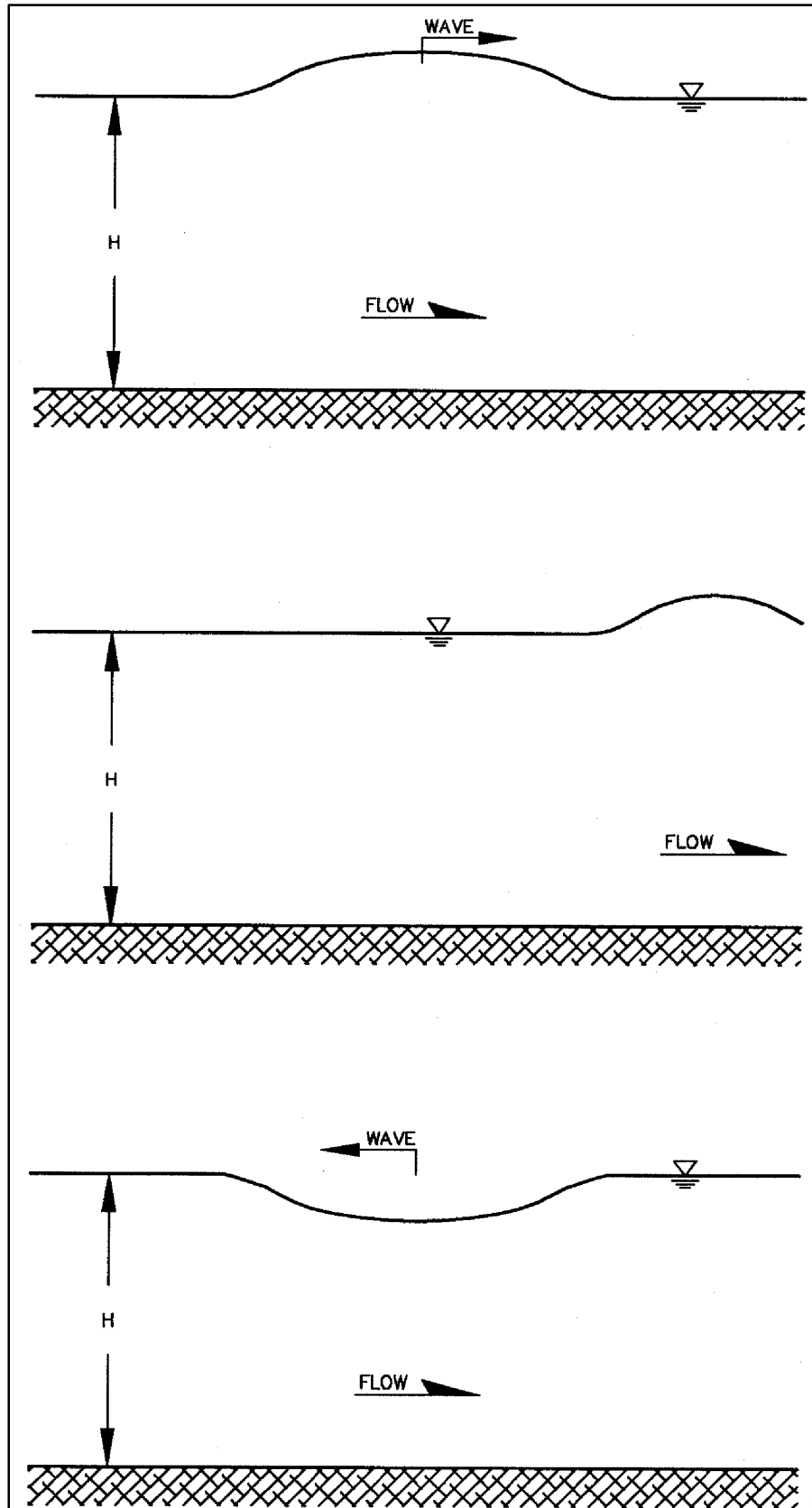


Figure 4. Solitary wave traveling into a reservoir

## Side Channels

A series of numerical experiments was conducted to assess the influence within secondary channels of forces generated by a vessel navigating the main channel. Geometric and hydraulic parameters used to describe the features of a river side channel are shown in Figure 5. Dimensional analysis of the representative terms  $l$ ,  $L$ ,  $B$ ,  $b$ ,  $D$ ,  $d$ ,  $V$ , and  $v$  leads to the geometric ratios  $L/l$ ,  $B/b$ , and  $D/d$ . Here,  $B/b$  and  $D/d$  describe a cross section and  $L/l$  describes the island length. Appropriate values of these descriptive ratios were determined from the Upper Mississippi River Database for Pool 8. Island lengths ( $L/l$ ) vary from 3.6 to 10, so a range of island-to-vessel length ratios of 2 to 10 were modeled. Secondary channel widths ( $b/B$ ) were found to vary only between 0.2 and 0.3, so the secondary-channel-to-main-channel width ratio was held constant at 0.25. Secondary channel depths ( $d/D$ ) vary from 0.4 to 0.9. A range of main channel depth from 1 to 3 times the secondary channel depth was simulated.

The main channel cross section for these experiments was similar to that found at Kampsville (Plate 3). Specifically, the main channel was 306.48 m wide with a maximum depth of 4.67 m. The thalweg was located 125.54 m from the right bank. The sailing line was 1.5 m left of the thalweg.

The vessel configuration was 297.2 m long by 32.0 m wide, drafted at 2.74 m. This represented a 3-wide by 5-long barge train. The tow traveled at 2.9 m/sec.

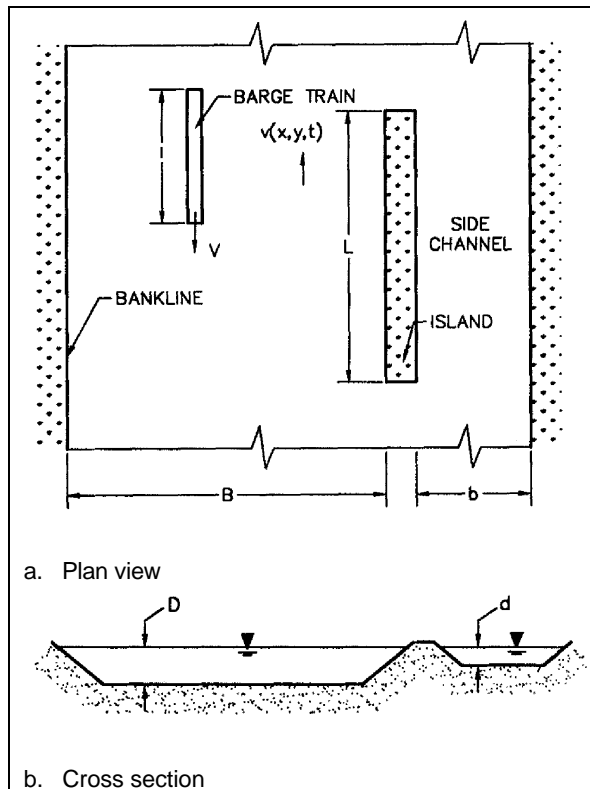


Figure 5. Geometric and hydraulic parameters describing side channels

Ambient conditions for each test were still water since vessel effects on the flow field are the interest in this study. The model parameters used for these experiments are provided in the following tabulation. Each simulation accelerated the vessel from rest to terminal speed (2.9 m/sec) in about 10.3 sec.

Schematics of the various geometries modeled and the corresponding time-histories of drawdown and current changes in the main channel and at the inlet, middle, and outlet of the secondary channel are shown in Plates 30-109. The zero abscissa is the time at which the bow of the vessel reaches the x-coordinate of the node plotted. The x-component of velocity is positive in the direction of the travel of the boat. The y velocity component is positive if it is directed into the side channel. At the entrance, the y velocity components are indicators of flow into the side channels.

Model Parameter	Value
$g, \text{ m/sec}^2$	9.81
$n$	0.025
$C$	0.1
$A, \text{ m/sec}^2$	0.2828
$T_s, \text{ sec}$	10.2552
$\beta$	0.25
$\alpha$	1.5
$\Delta t, \text{ sec}$	5.128

The x-component is simply the return currents produced by the vessel. This discussion will focus on flow in the side channel rather than the return currents.

Side channels behave somewhat differently from backwaters. The depression caused by the vessel will depress the water surface at the side channel entrance initially, but thereafter, the entrance behaves like a reservoir, i.e., the water surface remains fixed. In fact, both ends of the side channel are reservoirs. So the initial depression pulse will travel to the opposite end of the side channel where it will be negatively reflected and return as a positive wave. When this positive wave reaches the original end, it will be negatively reflected again and return as a depression. A complete cycle has a period of approximately  $2L/(gH)^{1/2}$ . Note that at all times the velocity pulse is directed toward the entrance where the vessel originally passed. Velocities at the ends of the side channels are amplified and so are typically larger than the velocities within the side channels. The vessel will continue to move along the river, passing the other inlet of the side channel. The velocity pulse produced at this inlet will tend to cancel those generated when the vessel passed the first inlet to the side channel. So in many of these examples one will see a fairly regular velocity-wave pattern until the vessel has time to reach the opposite channel end. At this point the velocity wave magnitude will reduce and appear to have shorter wave periods.

## Backwaters

Backwater parameters are displayed in Figure 6. The backwater plan shape was represented as a straight channel. Dimensionless parameters include the width of the channel into the backwater area ( $b/B$ ), the measure of the backwater area length ( $L/l$ ), and the measure of the backwater area depth ( $d/D$ ). Two backwater-to-vessel length ratios ( $L/l = 1$  and  $10$ ) were examined. Two different backwater entrance widths were simulated. The main-channel-to-backwater entrance width ratios ( $B/b$ ) of  $2$  and  $10$  were simulated. Main-channel-to-backwater-depth ratios ( $D/d$ ) were varied from  $1$  to  $4$ . Sketches of these geometries followed by the corresponding time-histories of the drawdown and currents generated by the vessel passage are shown in Plates 110-133. The main channel stations are located in the main channel

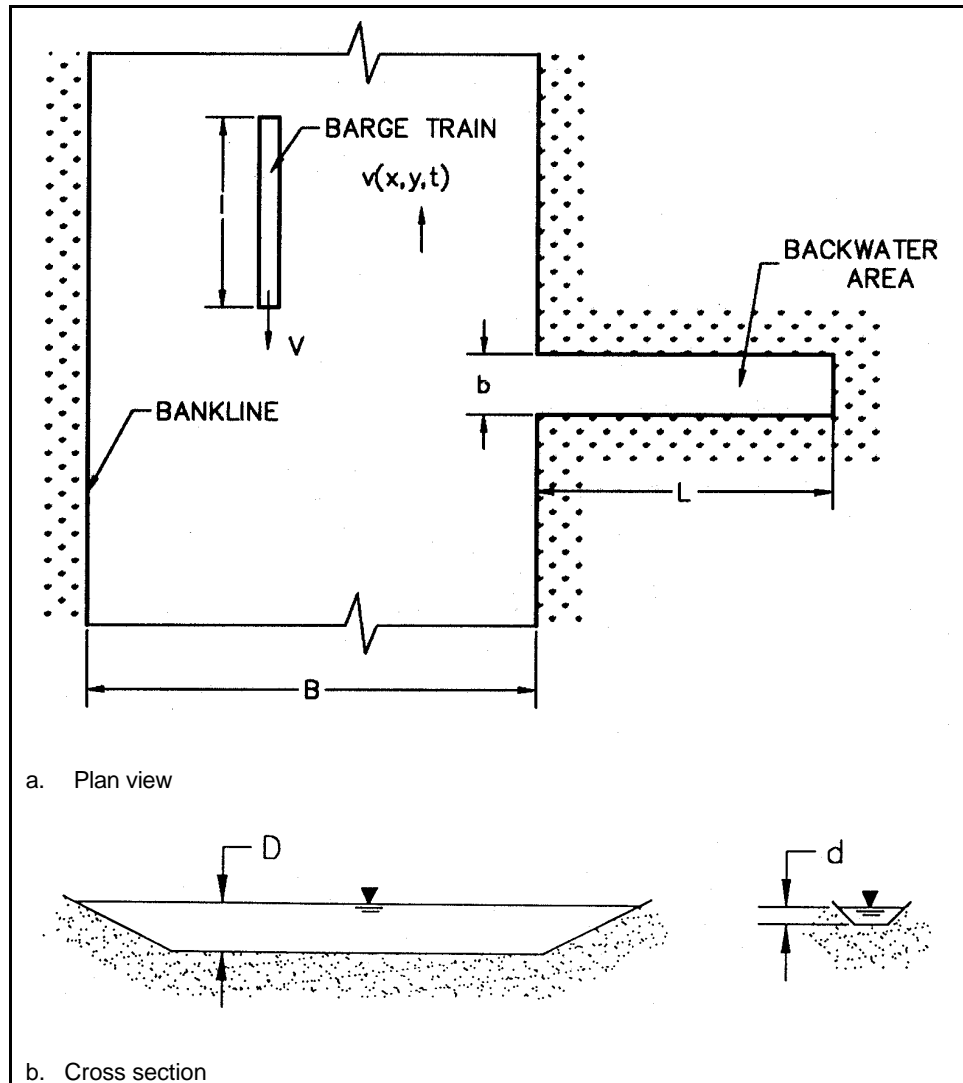


Figure 6. Geometric and hydraulic parameters describing backwaters

adjacent to the island center at a point one-half the distance from the sailing line to the island.

The depression caused by this vessel-generated pulse in a backwater initially causes a pulse of flow from the backwater channel into the main stem. This depression travels upstream until it is reflected off the closed end of the backwater. The reflected pulse is a depression, but the velocity is now directed into the backwater, toward the closed end. This reflected wave will then travel to the main stem. When the wave reaches the main stem, the junction of the main stem and backwater behaves like a reservoir so that the water surface will remain a constant but the velocities will be amplified. In some cases, the results will show larger velocity magnitudes at this point than from the initial drawdown velocity. So the reflection at the junction of the main stem and the backwater represents an overshoot in which the reflection of the depression wave is a positive wave traveling back into the

backwater. A complete cycle requires the wave to travel the length of the backwater channel four times. This is a period of  $4L/(gH)^{1/2}$ , where  $L$  is the channel length. The sum of the wave and its reflection produces a standing wave in the backwater. Here the water surface through the backwater will rise and fall in phase. The velocity will be out of phase with the water-surface wave. This is apparent in the plates for the backwater with length  $L/l = 1$ . The largest velocity amplitude is found at the entrance, and the largest water-surface amplitude is at the closed end of the backwater.

# 6 Discussion and Conclusions

---

## Discussion

The numerical model is an effective tool for quantifying the flow conditions in a navigation channel due to a moving tow traveling a predetermined sailing line. Velocities and water-surface fluctuations calculated using the depth-averaged flow equations provide a detailed determination of the magnitude and distribution of the flow field. Time-history comparisons capture the magnitude, flow reversals, and timing of these phenomena.

Advantages of this method over traditional one-dimensional analytical approaches for the quantification of tow-induced current and drawdown are many. Solution of the energy and continuity equations, as presented by Jansen and Schijf (1953), provides only a cross-sectional average return current and drawdown at midship in a uniform channel. The numerical model generates wave movement and gradients in two dimensions in a channel of arbitrary shape. The numerical model can be used to evaluate scenarios that are difficult to measure in the field or in a physical model. These scenarios include two tows passing and tows navigating channel bends. Finally, the numerical model provides visualization products that enable understanding of the complicated effects produced by vessels moving in a navigation channel.

## Conclusions

The model is limited to flows that are adequately described by the shallow-water equations; that is, three-dimensional flow near the vessel, where the vertical accelerations are significant, is not simulated. Vertical acceleration beneath the bow and stern may be so great that the shallow-water model is not applicable to the flow beneath the vessel. Another limitation of shallow-water models is that they cannot simulate short-period waves composing the divergent and stern wave field produced by a moving vessel. Also, no attempt has been made to reproduce the effects of a towboat propeller jet.

The shallow-water equations coupled with a moving pressure field representing the displacement of a vessel effectively model the far-field (area greater than about 2 to 2.5 vessel widths from the sailing line) currents and drawdown produced by a tow in an irregular channel section. The results of the "blind" tests comparing the physical model and prototype measurements to the numerical model calculations support this conclusion.

# References

---

- Abbott, M. B. (1979). *Computational hydraulics, elements of the theory of free surface flows*, Pitman Advanced Publishing Limited, London, 43.
- Berger, R. C. (1993). "A finite element scheme for shock capturing," Technical Report HL-93-12, U.S. Army Engineer Waterways Experiment Station, Vicksburg, MS.
- Berger, R. C., and Stockstill, R. L. (1995). "Finite-element model for high-velocity channels," *Journal of Hydraulic Engineering* 121(10), 710-716.
- Bhowmik, N. G., Soong, T. W., and Xia, R. (1993). "Physical effects of barge tows on the Upper Mississippi River System: Analysis of existing data collected by the Illinois Water Survey from the Kampsville Site on the Illinois River," Draft Progress Report No. 2, Illinois State Water Survey, Champaign, IL.
- \_\_\_\_\_. (1994). "Physical effects of barge tows on the Upper Mississippi River System: Analysis of existing data collected by the Illinois water survey from the Clark's Ferry site on the Mississippi River," Draft Progress Report, Illinois State Water Survey, Champaign, IL.
- Brater, E. F., and King, H. W. (1976). *Handbook of hydraulics for the solution of hydraulic engineering problems*. McGraw-Hill, New York. 7-17.
- Chapman, R. S., and Kuo, C. Y. (1985). "Applications of the two-equation  $k-\epsilon$  turbulence model to a two-dimensional, steady, free surface flow problem with separation," *International Journal for Numerical Methods in Fluids* 5, 257-268.
- Jansen, P. Ph., and Schijf, J. B. (1953). *18th International navigation congress*, Rome. Permanent International Association of Navigation Congresses, Brussels, Section 1, Communication 1, 175-197.
- Katopodes, N. D. (1986). "Explicit computation of discontinuous channel flow," *Journal of Hydraulic Engineering*, ASCE, 112(6), 456-475.

- Maynard, S. T. (1996). "Return velocity and drawdown in navigable waterways," Technical Report HL-96-7, U.S. Army Engineer Waterways Experiment Station, Vicksburg, MS.
- Maynard, S. T., and Martin, S. K. (1997). "Interim Report for the Upper Mississippi River - Illinois Waterway System Navigation Study, Physical Forces Study, Kampsville, Illinois Waterway," ENV Report 3, U. S. Army Engineer Waterways Experiment Station, Vicksburg, MS.
- Maynard, S. T., and Martin, S. K. (1998). "Interim Report for the Upper Mississippi River - Illinois Waterway System Navigation Study, Physical Forces Study, Clark's Ferry, Mississippi River," ENV Report 5, U. S. Army Engineer Waterways Experiment Station, Vicksburg, MS.
- Maynard, S. T., and Siemsen, T. S. (1991). "Return velocities induced by shallow-draft navigation." *Hydraulic Engineering: Proceedings of the 1991 National Conference*, Nashville, TN, July 29 – August 2, 1991. R. M. Shane, ed., ASCE, New York, 894-899.
- Rodi, W. (1980). "Turbulence models and their application in hydraulics - a state of the art review," State-of-the art paper, International Association for Hydraulic Research, Delft, The Netherlands.
- Stockstill, R. L., and Berger, R. C. (1994). "HIVEL2D: a two-dimensional flow model for high-velocity channels," Technical Report REMR-HY-12, U.S. Army Engineer Waterways Experiment Station, Vicksburg, MS.
- Stoker, J. J. (1957). *Water waves, the mathematical theory with applications*. Interscience Publishers, New York, 219-243.
- Whitham, G. B. (1974). *Linear and nonlinear waves*. John Wiley, New York, 462.